ACES Asian Chemical Editorial Society

doi.org/10.1002/cnma.202500020

CHEMNANOMAT
Research Article

www.chemnanomat.org

Synthesis and Characterization of Magnetic Cerium Oxide-Iron Oxide Hybrid Nanoparticles for Reactive Oxygen Species Production

Merve İlgar, David J. Morgan, Eun Byoel Kim, Igor L. Bolotin, and Preston T. Snee*

Cerium oxide nanoparticles (NPs) have excellent redox properties that enable biomedical functionalities. Similarly, magnetic NPs are emerging as important materials in related areas such as magnetic resonance imaging. Reported here are procedures to synthesize cerium oxide–iron oxide hybrid nanoparticles (CINPs) through the high-temperature thermal decomposition of metal oleate precursors. Varying both the temperature and relative precursor ratios avoided the formation of Fe_3O_4/CeO_2 Janus-like NPs, rather, the CINPs have a blended cerianite–magnetite structure. The potential for utilization of CINPs for various bio-applications such as photodynamic therapy and magnetic resonance imaging applications are demonstrated.

1. Introduction

Nanomaterials are highly efficient for a variety of applications because both the chemical compositions and structural morphologies can be tuned over a wide range. For example, the magnetic, optical, and electrical characteristics of metal oxide nanoparticles can be controlled through synthetic means.[1] Surface modifications are also facile, and in fact are generally necessary to enable functionality in various biomedical applications such as magnetic resonance imaging, targeted drug delivery, biosensing, bioseparation, and tissue engineering.[2–7] In this regard magnetite (Fe_3O_4) and maghemite (γ-Fe_2O_3) iron oxide nanoparticles (IONPs) ranging in size from 3 to ≈100 nm[8–11] have been extensively studied due to their excellent biocompatibility.[12–14] They have size tunable magnetic properties and express both chemical stability and low toxicity under physiological conditions.

Blending IONPs with cerium oxide nanoparticles (CONPs) is of interest[15] due to the latter's antioxidant properties that arise due to their oxygen affinity, redox properties, environmental impact, and surface chemistry.[16–18] CONPs are hard, radiation tolerant high bandgap luminescent materials with a fluorite crystal structure.[19,20] The complex surface chemistry of CONPs enable either the production or scavenging of reactive oxygen species (ROS)[21] depending on local environmental factors (e.g., pH).[22–24] For example, CONPs can exhibit superoxide dismutase-like activity by converting superoxide to hydrogen peroxide, the accumulation of which increases toxicity and enables anti-cancer radiotherapies.[25,26] Conversely, CONPs with a high proportion of surface Ce^{4+} can act as a catalase mimic and scavenge peroxide.[27] In the context of radiotherapy applications, the multifaceted redox chemistry of CONPs allow them to induce cancer cell death while simultaneously protecting healthy tissue from radiation-induced damage and oxidative stress.[25,28] As such, cerium oxide nanoparticles play an important role in bio-applications such as photodynamic therapy (PDT) for the selective destruction of targeted damaged cells.[29]

CONPs and IONPs are frequently synthesized via aqueous co-precipitation[30,31] or hydrothermal methods,[32–34] sol–gel,[35] or by high-temperature decomposition of metal oleate precursors in the presence of surfactants that impart colloidal stability and enable size control.[8,36–38] The latter method often renders hydrophobic products that require surface modification for biological applications.[39–42]

Core/shell and Janus structures of various metal oxide nanoparticles can be synthesized to realize new multifunctional hybrid nanostructures.[15,43] Additionally, solid solutions can create new materials with different properties, such as cerium orthoferrite ($FeCeO_3$) that has enhanced oxidation reactivity. Reported here is the synthesis of cerium oxide-iron oxide hybrid nanoparticles (CINPs), where the colloidal synthetic approach created a novel blend of Fe_3O_4 and CeO_2, as opposed to conjoined Janus, core/shell nanoparticles, or solid solutions. The CINPs display both the magnetic properties of magnetite and the ROS production capabilities of ceria, which enable applications as contrast agents and ROS agents in photodynamic therapy.[44]

M. İlgar
Department of Chemistry
Istanbul University-Cerrahpasa, 34320
Istanbul, Avcılar, Turkey

D. J. Morgan
Cardiff Catalysis Institute
School of Chemistry
Cardiff University
Cardiff CF24 4HQ, UK

E. B. Kim, I. L. Bolotin, P. T. Snee
Department of Chemistry
University of Illinois
Chicago 845 W, Taylor St., Chicago, Illinois 60607, USA
E-mail: sneep@uic.edu

Supporting information for this article is available on the WWW under https://doi.org/10.1002/cnma.202500020

2. Results and Discussion

Nanoparticles of iron oxide (IONPs), cerium oxide (CONPs), and iron/cerium oxide blends (CINPs) were prepared and characterized by a variety of methods. First, IONPs synthesized at 275 °C, 300 °C, and 325 °C were examined using Fourier transform infrared spectroscopy (FTIR) spectroscopy as shown in **Figure 1**A. All species display peaks in the 500 → 580 cm^{-1} range, which is indicative of Fe-O vibrations.[45] Furthermore, this resonance slightly blue shifts with increasing preparation temperature, which is indicative of a transformation from Fe_2O_3 to a Fe_3O_4 (magnetite) phase. The IONPs prepared at lower temperatures have bands at 1217, 1365 and 1738 cm^{-1} that appear to be either red- or blue-shifted oleic acid features, although we note that there is minimal consensus in the literature as per the structure and assignments of the FTIR spectra of IONPs. The IONP-325 FTIR spectrum is missing these features, and instead has 800 and 905 cm^{-1} peaks as well as a broad 1020 →1090 cm^{-1} feature that are likely due to Fe-OH surface species.[46] Overall, these data suggest that the surface passivation of IONPs is highly dependent on the synthesis temperature. The results of X-ray diffraction (XRD) analysis shown in Figure 1B reveal a small Fe_2O_3 (hematite) component in the IONP-275 sample; however, the characteristic peaks of the cubic magnetite Fe_3O_4 phase at 2θ = 30.1° (220), 35.5° (311), 43.1° (400), 57.0° (511), and 62.6° (440) are overall dominant.[47] Note that magnetite is a better fit to the data than the closely related γ-Fe_2O_3 (maghemite) structure. The narrow peaks observed in the XRD suggest large crystalline materials, which is consistent with the transmission electron microscopy (TEM) image of IONPs shown in Figure 1C that reveal rectangular-shaped particles over a 6 → 36 nm size range. Higher resolution TEM images shown in Figure S2 of the Supporting Information reveal lattice fringes at 0.51 (111)0.31 (220), 0.26 (311), and 0.15 nm (440), consistent with the cubic magnetite phase. The sum of these characterizations suggests that the synthesis at 325 °C resulted in a greater conversion of the iron oleate into the iron oxide (magnetite vs hematite) product, and that the synthesis temperature is also responsible for differences of surface passivation (oleate vs hydroxide). What is curious is that the homogeneity of particles in size and shape is suboptimal compared to previous reports using similar protocols that employed sodium oleate as a precursor.[8,11] Thus, despite the greater solubility of potassium in organic solvents, the use of the sodium salt appears to confer greater size homogeneity.

The FTIR spectra of CONP samples synthesized at 185 °C, 225 °C, and 265 °C are shown in Figure 1D. The two intense peaks at 2920 and 2850 cm^{-1} can be attributed to the symmetric and asymmetric C—H stretch oleate —CH_2 groups, as well as the peak at 721 cm^{-1} that represents the rocking mode.[48] Additionally, the broad features centered at 1430 cm^{-1} are found in the oleic acid, cerium oleate, and the CONP nanoparticle spectra. The 1535 cm^{-1} peak has been attributed to carboxylates binding to the CeO_2 surface;[49] other features seen in Figure 1D have been observed in previous studies.[50] Overall, the FTIR results suggest the successful preparation of ceria materials that are coated by oleate, albeit perhaps with a low reaction yield. The XRD spectra of CONPs samples are provided in Figure 1E. The width of the diffraction peaks suggests that either the materials are very small or amorphous (or both), which isn't improved by growth at higher temperatures. The TEM micrograph shown in Figure 1F and S3, Supporting

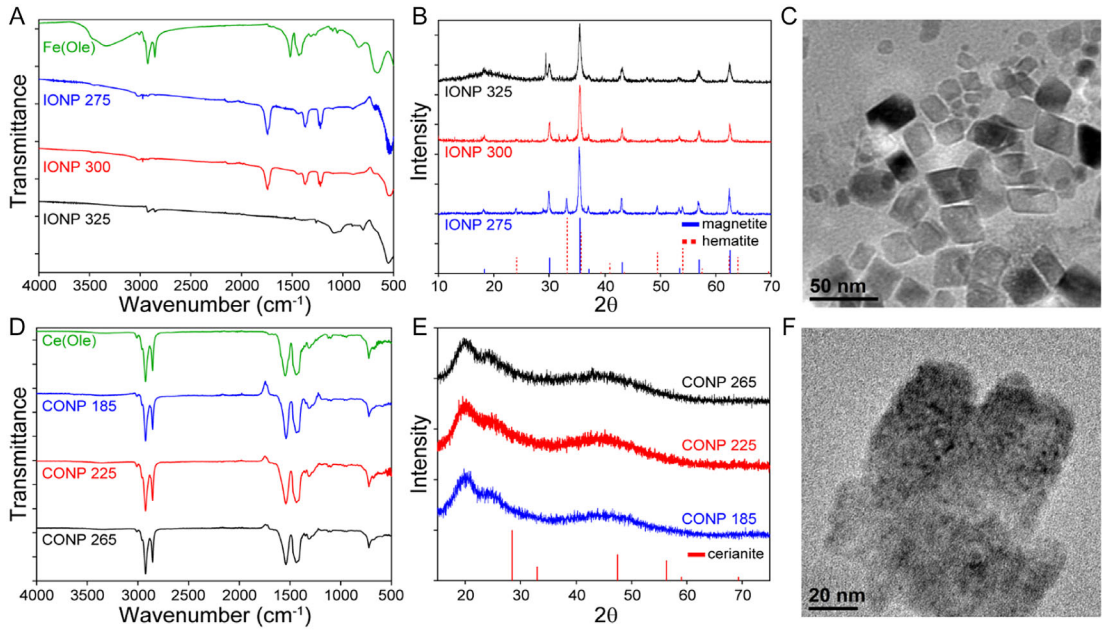

Figure 1. A) FTIR spectra of fe(Ole)$_3$ and various IONPs reveal decomposition of the iron oleate starting material into NP products. B) XRD of IONPs largely conform to the magnetite structure. Some hematite features are observed in the sample prepared at 275 °C. C) TEM of IONP-325 reveal large, somewhat heterogeneous particles, which is consistent with the sharp XRD resonances. D) FTIR spectra of Ce(Ole)$_3$ and various CONPs are very similar, indicating perhaps a low yield of CeO_2 NPs. E. XRD diffractograms of various CONP samples reveal a lack of crystallinity. F) TEM image of an amorphous ≈20 nm CONP particle suggests the broad XRD features is due to a lack of long-range crystallinity.

Information, distinguished between these possibilities as ≈5 → 20 nm particulates are observed with minimal discernable lattice fringes, which leads to the conclusion that the ceria NPs are largely amorphous. It is notable that it is difficult to obtain phase pure CeO_2 due to cerium's redox chemistry, potential for multiple crystal structures, and the fact that hydrates can affect the crystallinity of the solid state material.[51]

CINP nanoparticles were prepared by thermal decomposition of cerium and iron oleate at 325 °C. The FTIR data of the samples prepared with 5:1 and 9:1 $Ce(Ole)_3$ to $Fe(Ole)_3$ precursor ratios shown in **Figure 2**A are very similar to the CONPs. The carboxylate peaks from CONPs located at 1540 and 1430 cm^{-1} shift slightly, and a Fe—O metal–oxygen bond vibration peak is observed over the 585 → 570 cm^{-1} range for all the CINP samples. This peak is most prominent in the 2:1 cerium to iron oleate precursor ratio sample. XRD diffractograms of all the CINPs are shown in Figure 2C. Despite synthesis at 325 °C, the temperature at which IONPs fully realize magnetite crystallinity, the CINP XRD patterns are relatively muted, which implies less crystallinity. Furthermore, what features are discernable cannot be fully attributed to Fe_2O_3, Fe_3O_4, CeO_2, $CeFeO_3$ (perovskite), $CeFe_2O_5$, or $Ce_3Fe_5O_{12}$. We propose that CINP structures are best characterized as a distortion of an underlying Fe_3O_4 crystal structure. This is based on the fact that the CINP:2-1 pattern is most closely matched to magnetite, albeit at higher d-spacings, and the fact that the XRD peaks of CINP:5-1 further shift to higher d-spacings. These shifts can be attributed to a lattice expansion due to the inclusion of larger cerium ions.[52–55] For example, the strong 2θ = 29° feature observed in the CINP-5:1 diffractogram may originate from the 220 (2θ = 30.1°) lattice plane of Fe_3O_4. These XRD data are complemented by electron microscopy; for example, the TEM data of the CINP-5:1 shown in Figure 2D reveal lattice fringes of ≈0.31 nm periodicity are observed which corresponds to the intense 2θ = 29° XRD feature. At the same time, the high-resolution TEM shown in Figure S4, Supporting Information, reveal 0.24 and 0.28 nm lattice spacings for CINP:5-1, which neither correspond to any XRD feature nor are not particularly assignable to any cerium or iron oxide, nor known admixtures of the two.

The inclusion of more cerium in the CINP-9:1 sample prepared at a high cerium to iron oleate precursor ratio results in a featureless XRD pattern. Furthermore, the CINP-9:1 NPs observed in Figures 2E and S5, Supporting Information, are ≈10 nm, which is large enough to provide reasonably sharp XRD peaks if the samples were crystalline, implying that these nanomaterials are amorphous structure. This is reflected in the fact that the high-resolution TEM images reveal particles with no observable lattice fringes for the most part, although in a few instances a 0.28 nm lattice spacing is observed that is assignable to the (200) lattice spacing of CeO_2.

While the XRD of CINP:5-1 can be attributed to a distortion of Fe_3O_4 by cerium ions, the same is not true for the CINP:9-1 sample due to its broad and near-featureless diffraction spectrum. As a result, XPS analyses were performed to characterize the elemental content. The survey spectra of all CINP samples shown in Figure 2B reveal cerium and iron peaks at *ca.* 885 and 710 eV, respectively. Unfortunately charging effects created uncertainty in the binding energy positions, which hampered precise chemical identification.

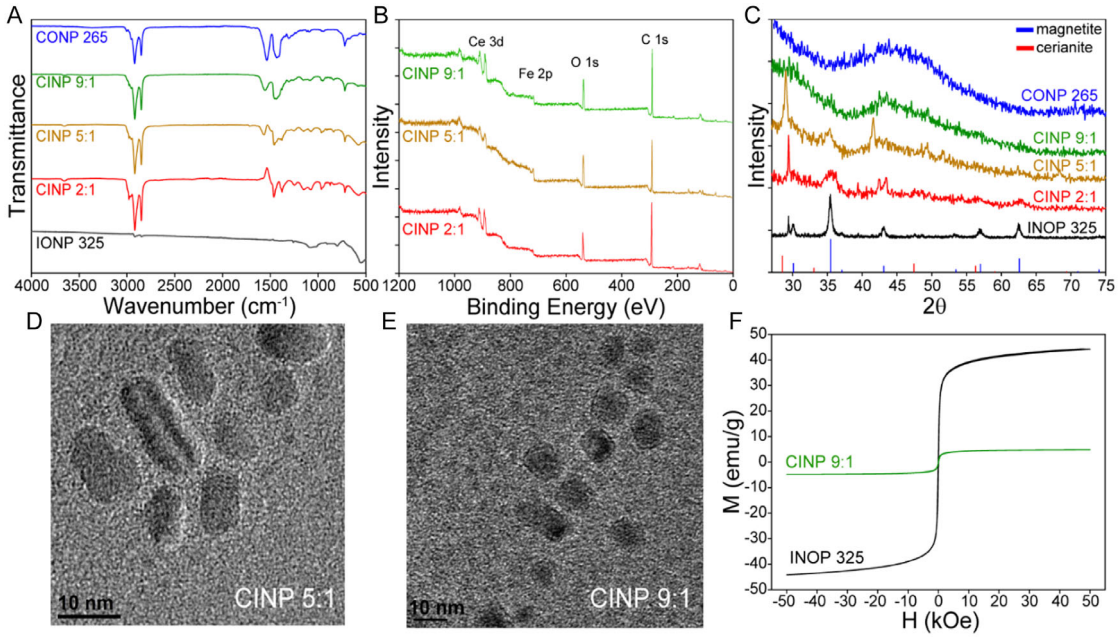

Figure 2. A) FTIR spectra of CINP NPs reveal a transition from a CONP to IONP features as a function of increasing iron content. B) XPS survey spectra of CINP samples reveal the presence of iron and cerium. C) XRD diffractograms of CINPs are best described as a distortion of an underlying magnetite phase that shifts due to a lattice expansion. D) TEM image of CINP-5:1 reveals polydisperse particles that vary in size from 5 → 15 nm. Lattice fringes are observed in some NPs. E) TEM of CINP-9:1 reveal ≈10 nm particles with minimal discernible crystallinity, which is consistent with XRD characterization. F) Vibrating-sample magnetometer characterization reveals superparamagnetic behavior in IONP-325 and CINP-9:1 NPs.

Regardless, the XPS spectra in the Ce3d region shown in Figure S6 of the Supporting Information appear to suggest a predominant Ce(III) composition, although the CONP sample may have some Ce(IV) content based on the broadness of the Ce3d$_{3/2}$ 900 eV feature.[38] The Fe 2p$_{3/2}$ region at ≈711 eV shown in Figure S6, Supporting Information, indicate the presence of Fe(III). The XPS data were used to determine the elemental composition as shown in Table S1, Supporting Information. Both the CINP-9:1 and CINP-2:1 reveal a ≈20% iron content while the CINP-5:1 was ≈50%. As a result, the XPS results are not correlated to the preparation conditions, which may simply be due to the presence of excess cerium or iron due to inefficient processing (this problem has hampered characterization of other metal chalcogenide nanomaterials, see ref. [56]). Regardless, the cerium and iron content must originate from the same nanomaterials, otherwise the phase-pure particles would have been discernable in the XRD patterns. The carbon and oxygen peaks (285 and 530 eV, respectively) likely originate from the substrate and oleic acid ligands.

Magnetic properties were characterized using a vibrating-sample magnetometer (VSM) to examine the iron oxide content of the CINP samples. The VSM profiles for IONP-325 and CINP-9:1 shown in Figure 2F reveal the absence of a hysteresis loop and minimal coercivity, which is consistent with super paramagnetism.[51] The magnetization value of IONPs was found to be 42 emu g^{-1}, which decreased with increasing cerium content. Specifically, the CINP-9:1 magnetization of 4.7 emu g^{-1} was ≈9-fold less than the pure IONP and correlates to the stoichiometry of the cerium to iron oleate precursor ratio. At the same time, the CINP's magnetic properties are significantly greater than observed with CeO_2, which is formally diamagnetic yet NPs do show some ferromagnetism due to surface chemistry effects via oxygen vacancies.[57]

As IONPs are not well known for photochemical generation of ROS, the ability of CINPs to retain photochemical ROS generation capability was investigated. To this end the CINP-9:1 sample was first water solubilized using 40% octylamine-modified poly(acrylic acid) and then tested for the photochemical generation of ROS by the quenching of p-nitrosodimethylaniline absorption in the presence of imidazole. This test was applied due to the sensitivity for the presence of hydroxyl radicals, which are expected to be produced by CeO_2 and Fe_3O_4 NPs.[58–60] Additionally, the CINP 9:1 sample was applied to minimize the potential for free iron to instigate Fenton-type chemistry that produced hydroxy radicals.[59] Note that the polymer-encapsulation mechanism is well-established and confers stability to erstwhile hydrophobic NPs;[61–63] furthermore, encapsulation does not significantly impede photochemical catalysis.[64] Figure S7, Supporting Information, shows the concentration dependent change in the ROS-reporting chromophore's absorbance as a function of UV irradiation exposure time. Integration of the dye absorption reveals quenching as a function of CINP-9:1 concentration as shown in **Figure 3**. Compared to a control, the dye quenching above a threshold concentration (0.04 mg mL^{-1} as seen in Figure 3) is greatly accelerated during photolysis in the presence of CINP, which we attribute to greater ROS generation and reveals the applicability of these hybrid nanostructures for use in PDT applications. Concerning the

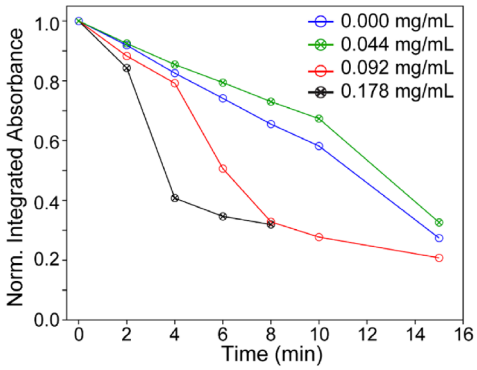

Figure 3. Time-dependent quenching of a reactive oxygen species (ROSs) sensing dye reveals the presence of ROS as the concentration of CINP-9:1 increases beyond a threshold of 0.044 mg mL^{-1} catalyst, which represents a threshold for detection using this mechanism.

mechanism of ROS production, the high content of Ce^{3+} indicates oxygen vacancies, which enables the photochemical generation of ROS such as superoxo and peroxo in water.[65] Furthermore, it is possible that superoxide can be converted to peroxide,[66] and for the iron oxide to convert the peroxide into hydroxy radicals.[58] Thus, it is possible that CeO_2/Fe_2O_3 hybrid materials have synergistic interactions that enhance the production of hydroxy radicals.[59,60] An additional dynamic concerns previous research with co-precipitated CeO_2/Fe_2O_3 composite nanospindles that found evidence for enhanced catalytic activity due to sequestration of electron and hole carriers between cerium and iron, respectively, which enhances the excited state lifetime.[67] The splitting of charge carriers enables each species to produce multiple ROS species such as hydroxyl radicals via oxidation and reduced superoxide anions, which has been observed in photochemical organic dye degradation[68–71] as well as in studies of the antimicrobial properties[72] of hydrothermal prepared co-precipitated CeO_2/Fe_2O_3 nanocomposites.

3. Conclusions

Colloidal IONPs and CONPs samples were synthesized using $Ce(Ole)_3$ and $Fe(Ole)_3$. While all cCONP samples were amorphous, the iron oxide achieved good magnetite crystallinity at a 325 °C growth temperature. For this reason, the same temperature was applied for the synthesis of cerium oxide-iron oxide NPs at various precursor ratios. XPS analyses revealed the presence of both iron and cerium, and both FTIR and XRD characterizations indicated the formation of a product best described as a hybrid of Fe_3O_4 and CeO_2 due to the presence of a distorted magnetite structure for samples prepared at a high iron to cerium ratio. The various CINP materials displayed the superparamagnetic characteristics of iron oxide nanoparticles coupled with the ROS generation capability of ceria. As a result, these hybrid nanostructures hold great potential for biomedical applications. For example, magnetic separation and/or guidance of these nanostructures is feasible, as well as acting as an MRI contrast agent. At the same time, the high Ce^{3+}

content of these materials engenders toxicity and enables many anti-cancer activities,[73,74] and as a photosensitizer in MRI and PDT applications, respectively.

4. Experimental Section

Chemicals and Materials

Cerium (III) chloride heptahydrate ($CeCl_3{\cdot}7H_2O$, 99%) and imidazole (99%) were purchased from Alfa Aesar, iron chloride hexahydrate ($FeCl_3 \cdot 6H_2O$, 97%), 1-octodecene (technical grade, 90%), oleic acid (technical grade, 90%) were obtained from Sigma–Aldrich, potassium hydroxide, 2-propanol (ACS), and ethanol were purchased from Fisher Chemical. Spectra/Por Float-A-Lyzer G2 dialysis tubes (300 kDa MWCO) were purchased from Millipore. N, N-Dimethyl-4-nitrosoaniline (98.0+%) was purchased from TCI America. Oleic acid was recrystallized prior to use while all the materials were used without further purification.

Synthesis of Metal Oleates: Iron Oleate

Into a 2-neck 250 mL round bottom flask was added 1.3515 g $FeCl_3 \cdot 6H_2O$ (5 mmol) with 5 mL D.I. water, which was stirred until dissolved. The flask was then heated to reflux in an oil bath. Next, 4.312 g of oleic acid (15 mmol) and 0.8415 g of potassium hydroxide (15 mmol) were dissolved into a solution of 10 mL ethanol, 2.5 mL distilled water, and 17 mL hexane that was next added dropwise into the stirring $FeCl_3$ solution. The solution was stirred under an N_2 atmosphere at 70 °C for 4 h. Afterwards, the solution was washed 4× with distilled water, after which the burgundy-brown organic layer was separated and dried. The remaining free oleic acid and by-products were removed by centrifugation (3× for 10 min at 3500 RPM) with isopropyl alcohol. Finally, the brown-orange precipitate that was separated by centrifugation was heat treated in an oil bath at 70 °C for 5 h.

Synthesis of Metal Oleates: Cerium Oleate

Into a 2-neck 250 mL round bottom flask was added 1.2324 g $CeCl_3$ (5 mmol) with 5 mL distilled water, which was stirred until dissolved. The flask was then heated to reflux in an oil bath. Next, 4.312 g oleic acid (0.015 mol) and 0.8415 g of potassium hydroxide (0.015 mol) were dissolved into a solution of 10 mL ethanol, 2.5 mL distilled water, and 17 mL hexane that was next added dropwise into the stirring $CeCl_3$ solution. The solution was stirred in an oil bath and under an N_2 atmosphere at 70 °C for 4 h. Afterwards, the solution was washed 4× with distilled water. The pale-yellow organic layer was separated and centrifuged (30 min at 3500 RPM) with isopropyl alcohol to remove excess oleic acid and by-products. The pale-yellow precipitate, separated by centrifugation, was dried under a vacuum for 4 h to obtain the final product.

The FT-IR spectra of oleic acid, $Fe(Ole)_3$, and $Ce(Ole)_3$ are shown in Figure S1 of the Supporting Information. Successful preparation of the metal oleate precursors was verified by the lack of the characteristic 1710 cm^{-1} band of free oleic acid.[75,76]

Synthesis of Metal Oleates: Synthesis of IONPs

Into a 50 mL 3-neck round bottom flask was added 0.0564 g recrystallized oleic acid (0.2 mmol), 0.18 g of $Fe(Ole)_3$ (0.2 mmol), and 10 mL of 1-octadecene. The flask was kept under vacuum for 30 min while stirring. Afterwards, the solution was heated to 275 °C under an N_2 atmosphere and held at that temperature for 20 min. Before characterization the IONPs were precipitated by addition of hexane and were isolated by centrifugation, followed by vacuum drying. IONPs were also prepared at 300 °C and 325 °C.

Synthesis of Metal Oleates: Synthesis of CONPs

Into a 3-neck 50 mL round bottom flask was added 0.0564 g oleic acid (0.2 mmol), 0.198 g of $Ce(Ole)_3$ (0.2 mmol), and 15 mL of 1-octadecene, which were mixed at 60°C until a homogeneous solution was obtained. Next, it was cooled to room temperature under vacuum over the course of 30 min. Afterwards, the flask was put under an N_2 atmosphere and was heated to 185 °C for 2 h. The CONPs were precipitated by isopropanol and isolated by centrifugation, followed by vacuum drying before characterization. CONPs were also prepared at 225 °C and 265 °C.

Synthesis of Metal Oleates: Synthesis of CINPs

For CINPs synthesized at a 2:1 molar cerium to iron ratio, first 0.0599 g $Fe(Ole)_3$ (0.0666 mmol) was added to 5 mL 1-octadecene in a glass vial. The iron oleate was mixed until dissolution, and the solution was then degassed under vacuum for 30 min and was subsequently stored under an N_2 atmosphere. Into a 3-neck 50 mL round bottom flask was added 0.0564 g oleic acid (0.2 mmol), 0.1316 g $Ce(Ole)_3$ (0.0133 mmol), and 10 mL 1-octadecene. The solution was mixed at 60 °C until homogeneous. Afterwards it was cooled to room temperature while under vacuum over the course of 30 min. Next, the flask was put under an N_2 atmosphere and was heated to 185 °C for 2 h, and then heated to 325 °C. The $Fe(Ole)_3$ solution was then rapidly injected into the flask, and the mixture was stirred for 20 min while maintaining the high temperature. The dark brown solution was processed by precipitation with isopropanol followed by isolation by centrifugation. The solids were dried under vacuum before characterization. The same process was repeated at 5:1 and 9:1 $Ce(Ole)_3$ to $Fe(Ole)_3$ precursor ratios.

Synthesis of Metal Oleates: Preparation of Water Solubilized CINPs

The polymer encapsulating agent 40% octylamine-modified poly(acrylic acid) was prepared according to literature procedures.[40,61] A 0.74 g portion of the CINP-9:1 in growth solution was processed by dissolution in hexane followed by precipitation via the addition of a co-solvent (isopropanol) and then a non-solvent (methanol) in several cycles. A solid pellet was isolated by centrifugation and then dried; typically, 15 mg was obtained. Next, the pellet was dissolved in chloroform, followed by addition of 50 mg of 40% octylamine modified poly(acrylic acid). After sonication to assure the polymer had dissolved, the chloroform was removed under vacuum, leaving a residue that was dissolved with ≈1 mL of a 0.1 M NaOH solution and diluted to a total of 10.8 mL with DI water. The sample underwent dialysis against DI water in a 300 kDa MWCO dialysis tube until the pH was neutral.

Synthesis of Metal Oleates: Characterizations

Fourier transform infrared spectroscopy (FT-IR) analysis was performed with a Thermo Scientific Nicolet iS5 FT-IR Spectrometer incorporating an iD7 Diamond ATR with a resolution of 4 cm^{-1} over a 400–4000 cm^{-1} range. XRD analysis was performed with a Bruker

D8 Advance diffractometer with a Cu Kα radiation source (λ = 1.5418 Å) operating at 40 kV and 40 mA. TEM micrographs were obtained with a JEOL-JEM-3010 transmission electron microscope at 300 kV HT accelerating voltage at 0.14 nm resolution. X-ray photoelectron spectroscopy (XPS) was performed using a system built within the laboratory utilizing a monochromatic Al Kα X-ray source. Spectra were calibrated against an aliphatic C1s peak, taken to be 285 eV ($\pm$ 0.2 eV). Spectra were processed using CasaXPS. Vibrating sample magnetometry (VSM) was performed using Quantum Design PPMS-9 T to characterize the magnetic behavior of the samples at room temperature in the field range of $\pm$50 kOe.

ROS measurement. The capacity for CINP samples to photochemically generate ROS species (hydroxide radical, superoxo, and singlet oxygen) was evaluated by the absorptive quenching a chromophore as per the protocol of ref. [77]. A stock solution of an ROS sensing chromophore was prepared by dissolving 109 mg imidazole (1.6 mmol) with 1.5 mg (0.01 mmol) p-nitrosodimethylaniline dye in 100 mL DI water. Next, individual portions of a water-solubilized $\approx$1.5 mg mL^{-1} CINP-9:1 dispersion in water (0.156, 0.322, and 0.644 mL) were added with 1.611 g of the dye stock solution and diluted to a total of 5 mL with DI water. A control sample containing 5 mg of the water-solubilizing polymer was also prepared. The various samples including control were loaded into 5 mL quartz cuvettes (Starna Scientific) with a small stir bar and were tightly capped. The samples were placed in the air-cooled cavity of a Rayonet UV photolysis chamber for $\approx$1, 2, or 5 min intervals while stirring, followed by characterization by UV/Vis absorption spectroscopy with a Cary Bio 300. The Rayonet photolysis system was equipped with 16 $\times$ 8W UV light bulbs from Interlight (Hammond, IN).

Acknowledgements

Merve İlgar for conceptualization of experiments, data curation, formal analysis, and report preparation. D.J.M assisted with formal analysis of XPS data. E.B.K and I.L.B assisted with data curation of TEM and XPS. P.T.S was responsible for project administration, and assisted with data curation, formal analysis, and report preparation. Also we acknowledge Luke Hanley from University of Illinois Chicago for assistance with XPS analysis. M.İ would like to acknowledge the financial support from the Council of Higher Education-Overseas Doctorate Research Scholarship for Research Assistants (YÖK-YUDAB) and Istanbul University Cerrahpasa, Engineering Faculty, Chemistry Department. Also the University of Illinois Chicago for funding.

Conflict of Interest

The authors declare no conflict of interest.

Author Contributions

Merve İlgar: conceptualization (lead); data curation (lead); formal analysis (equal); writing—original draft (lead). **David J. Morgan**: formal analysis (equal). **Eun Byoel Kim**: data curation (supporting). **Igor L. Bolotin**: data curation (supporting). **Preston T. Snee**: formal analysis (lead); project administration (lead); writing—review & editing (lead).

Data Availability Statement

The data that support the findings of this study are available from the corresponding author upon reasonable request.

Keywords: cerium nanoparticles · reactive oxygen species · superparamagnetic iron oxide · theranostic

[1] M. S. Chavali, M. P. Nikolova, *SN Appl. Sci.* **2019**, *1*, 607.
[2] P. I. P. Soares, C. A. T. Laia, A. Carvalho, L. C. J. Pereira, J. T. Coutinho, I. M. M. Ferreira, C. M. M. Novo, J. P. Borges, *Appl. Surf. Sci.* **2016**, *383*, 240.
[3] K. Chen, X. Sun, Y. Liu, Y. Yang, M. Shi, J. Yu, S. Zhang, P. Shi, *Inorg. Chem.* **2022**, *61*, 16307.
[4] Y. Fan, P. Li, B. Hu, T. Liu, Z. Huang, C. Shan, J. Cao, B. Cheng, W. Liu, Y. Tang, *Inorg. Chem.* **2019**, *58*, 7295.
[5] H.-Y. Park, M. J. Schadt, I.-I. S. L. Wang, P. N. Njoki, S. H. Kim, M.-Y. Jang, J. Luo, C.-J. Zhong, *Langmuir* **2007**, *23*, 9050.
[6] O. Ziv-Polat, H. Skaat, A. Shahar, S. Margel, *IJN* **2012**, *7*, 1259.
[7] J. B. Haun, T.-J. Yoon, H. Lee, R. Weissleder, *Wiley Interdiscip. Rev. Nanomed. Nanobiotechnol.* **2010**, *2*, 291.
[8] N. R. Jana, Y. F. Chen, X. G. Peng, *Chem. Mater.* **2004**, *16*, 3931.
[9] P. Guardia, N. Pérez, A. Labarta, X. Batlle, *Langmuir* **2010**, *26*, 5843.
[10] P. Kucheryavy, J. He, V. T. John, P. Maharjan, L. Spinu, G. Z. Goloverda, V. L. Kolesnichenko, *Langmuir* **2013**, *29*, 710.
[11] J. Park, K. An, Y. Hwang, J.-G. Park, H.-J. Noh, J.-Y. Kim, J.-H. Park, N.-M. Hwang, T. Hyeon, *Nat. Mater* **2004**, *3*, 891.
[12] B. Chertok, B. A. Moffat, A. E. David, F. Yu, C. Bergemann, B. D. Ross, V. C. Yang, *Biomaterials* **2008**, *29*, 487.
[13] A. Figuerola, R. Di Corato, L. Manna, T. Pellegrino, *Pharmacol. Res.* **2010**, *62*, 126.
[14] F. Roohi, J. Lohrke, A. Ide, G. Schütz, K. Dassler, *IJN* **2012**, *7*, 4447.
[15] Y. Wu, Y. Yang, W. Zhao, Z. P. Xu, P. J. Little, A. K. Whittaker, R. Zhang, H. T. Ta, *J. Mat. Chem. B* **2018**, *6*, 4937.
[16] I. Rodea-Palomares, S. Gonzalo, J. Santiago-Morales, F. Leganés, E. García-Calvo, R. Rosal, F. Fernández-Piñas, *Aquat. Toxicol.* **2012**, *122-123*, 133.
[17] J. T. Dahle, Y. Arai, *Int. J. Environ. Res. Public Health* **2015**, *12*, 1253.
[18] A. Dhall, W. Self, *Antioxidants* **2018**, *7*, 97.
[19] Y. Sheng, L. Yang, H. Luan, Z. Liu, Y. Yu, J. Li, N. Dai, *J. Nucl. Mater.* **2012**, *427*, 58.
[20] B. Ye, M. A. Kirk, W. Chen, A. Oaks, J. Rest, A. Yacout, J. F. Stubbins, *J. Nucl. Mater.* **2011**, *414*, 251.
[21] C. Nathan, A. Cunningham-Bussel, *Nat. Rev. Immunol.* **2013**, *13*, 349.
[22] Y. Liu, Y. Wu, R. Zhang, J. Lam, J. C. Ng, Z. P. Xu, L. Li, H. T. Ta, *ACS Appl. Bio Mater.* **2019**, *2*, 5930.
[23] J. L. Y. Tang, S. S. Moonshi, H. T. Ta, *Cell. Mol. Life Sci.* **2023**, *80*, 46.
[24] F. Corsi, F. Caputo, E. Traversa, L. Ghibelli, *Front. Oncol.* **2018**, *8*, 309.
[25] M. S. Wason, J. Colon, S. Das, S. Seal, J. Turkson, J. Zhao, C. H. Baker, *Nanomed. Nanotechnol. Biol. Med.* **2013**, *9*, 558.
[26] E. G. Heckert, A. S. Karakoti, S. Seal, W. T. Self, *Biomaterials* **2008**, *29*, 2705.
[27] T. Pirmohamed, J. M. Dowding, S. Singh, B. Wasserman, E. Heckert, A. S. Karakoti, J. E. S. King, S. Seal, W. T. Self, *Chem. Commun.* **2010**, *46*, 2736.
[28] R. W. Tarnuzzer, J. Colon, S. Patil, S. Seal, *Nano Lett.* **2005**, *5*, 2573.
[29] Y. Li, J. Yang, X. Sun, *Front. Chem.* **2021**, *9*, 650587.
[30] J. Lee, T. Isobe, M. Senna, *J. Colloid Interface Sci.* **1996**, *177*, 490.
[31] M. Ramachandran, R. Subadevi, M. Sivakumar, *Vacuum* **2019**, *161*, 220.
[32] C. Korsvik, S. Patil, S. Seal, W. T. Self, *Chem. Commun.* **2007**, 1056.
[33] C. Sun, H. Li, H. Zhang, Z. Wang, L. Chen, *Nanotechnology* **2005**, *16*, 1454.
[34] J. Zdravković, B. Simović, A. Golubović, D. Poleti, I. Veljković, M. Šćepanović, G. Branković, *Ceram. Int.* **2015**, *41*, 1970.
[35] K. Suri, S. Annapoorni, R. P. Tandon, N. C. Mehra, *Synth. Met.* **2002**, *126*, 137.
[36] H. Imagawa, A. Suda, K. Yamamura, S. Sun, *J. Phys. Chem. C* **2011**, *115*, 1740.
[37] R. Álvarez-Asencio, R. W. Corkery, A. Ahniyaz, *RSC Adv.* **2020**, *10*, 14818.
[38] T. Yu, B. Lim, Y. Xia, *Angew. Chem., Int. Ed., Engl.* **2010**, *49*, 4484.
[39] A. G. Kurian, N. Mandakhbayar, R. K. Singh, J.-H. Lee, G. Jin, H.-W. Kim, *Mater. Today Bio.* **2023**, *20*, 100664.
[40] Y. Chen, R. Thakar, P. T. Snee, *J. Am. Chem. Soc.* **2008**, *130*, 3744.
[41] J. T. Duong, M. J. Bailey, T. E. Pick, P. M. McBride, E. L. Rosen, R. Buonsanti, D. J. Milliron, B. A. Helms, *J. Polym. Sci., Part A: Polym. Chem.* **2012**, *50*, 3719.

[42] I. Robinson, C. Alexander, L. D. Tung, D. G. Fernig, N. T. K. Thanh, *J. Magn. Magn. Mater.* **2009**, *321*, 1421.
[43] H. Ding, Y. Zhao, Q. Duan, J. Wang, K. Zhang, G. Ding, X. Xie, C. Ding, *J. Rare Earth.* **2017**, *35*, 984.
[44] T. Lammers, S. Aime, W. E. Hennink, G. Storm, F. Kiessling, *Acc. Chem. Res.* **2011**, *44*, 1029.
[45] V. Vilas-Boas, N. Guldris, E. Carbó-Argibay, D. G. Stroppa, M. F. Cerqueira, B. Espiña, J. Rivas, C. Rodríguez-Abreu, Y. V. Kolen'ko, *RSC Adv.* **2015**, *5*, 47954.
[46] X. Huang, A. Schmucker, J. Dyke, S. M. Hall, J. Retrum, B. Stein, N. Remmes, D. V. Baxter, B. Dragnea, L. M. Bronstein, *J. Mater. Chem.* **2009**, *19*, 4231.
[47] B. Wechsler, D. Lindsley, C. Prewitt, *Am. Min.* **1984**, *69*, 754.
[48] M. Unger, D. Chaturvedi, S. Mishra, P. Tandon, H. W. Siesler, *Spectrosc. Lett.* **2013**, *46*, 21.
[49] F. Dang, K. Kato, H. Imai, S. Wada, H. Haneda, M. Kuwabara, *Cryst. Growth Des.* **2010**, *10*, 4537.
[50] J. Saranya, B. S. Sreeja, G. Padmalaya, S. Radha, T. Manikandan, *J. Inorg. Organomet. Polym.* **2020**, *30*, 2666.
[51] R. F. André, G. Rousse, C. Sassoye, M. Avdeev, B. Lassalle-Kaiser, B. Baptiste, S. Carenco, *Chem. Mater.* **2023**, *35*, 5040.
[52] F. J. Pérez-Alonso, M. López Granados, M. Ojeda, P. Terreros, S. Rojas, T. Herranz, J. L. G. Fierro, M. Gracia, J. R. Gancedo, *Chem. Mater.* **2005**, *17*, 2329.
[53] F. J. Pérez-Alonso, M. L. Granados, M. Ojeda, T. Herranz, S. Rojas, P. Terreros, J. L. G. Fierro, M. Gracia, J. R. Gancedo, *J. Phys. Chem. B* **2006**, *110*, 23870.
[54] F. J. Perez-Alonso, I. Melián-Cabrera, M. López Granados, F. Kapteijn, J. L. G. Fierro, *J. Catal.* **2006**, *239*, 340.
[55] Z. Gu, K. Li, S. Qing, X. Zhu, Y. Wei, Y. Li, H. Wang, *RSC Adv.* **2014**, *4*, 47191.
[56] A. M. Jawaid, D. J. Asunskis, P. T. Snee, *ACS Nano* **2011**, *5*, 6465.
[57] A. Sundaresan, C. N. R. Rao, *Nano Today* **2009**, *4*, 96.
[58] L. Xu, J. Wang, *Appl. Catal. B: Environ.* **2012**, *123-124*, 117.
[59] L. Xu, J. Wang, *Environ. Sci. Technol.* **2012**, *46*, 10145.
[60] Y. Sun, L. Xu, X. Liu, Y. Shen, Y. Zhang, N. Gu, F. Xiong, *Chem. Eng. J.* **2022**, *429*, 132303.
[61] X. Y. Wu, H. J. Liu, J. Q. Liu, K. N. Haley, J. A. Treadway, J. P. Larson, N. F. Ge, F. Peale, M. P. Bruchez, *Nat. Biotechnol.* **2003**, *21*, 41.
[62] C. M. Tyrakowski, P. T. Snee, *Phys. Chem. Chem. Phys.* **2014**, *16*, 837.
[63] F. Lisi, J. Sawayama, S. Gautam, S. Rubanov, X. Duan, N. Kirkwood, *ACS Appl. Nano Mater.* **2023**, *6*, 4046.
[64] M. T. Fortunato, J. M. O'Shea, J. Huang, H. Chandrasiri, E. B. Kim, A. M. Jamhawi, A. J.-L. Ayitou, P. T. Snee, C. Turro, *Nanoscale* **2025**, *17*, 3837.
[65] G. Preda, A. Migani, K. M. Neyman, S. T. Bromley, F. Illas, G. Pacchioni, *J. Phys. Chem. C* **2011**, *115*, 5817.
[66] A. A. Fauzi, A. A. Jalil, N. S. Hassan, F. F. A. Aziz, M. S. Azami, I. Hussain, R. Saravanan, D.-V. N. Vo, *Chemosphere* **2022**, *286*, 131651.
[67] N. S. Arul, D. Mangalaraj, R. Ramachandran, A. N. Grace, J. I. Han, *J. Mater. Chem. A* **2015**, *3*, 15248.
[68] W. A. Aboutaleb, R. A. El-Salamony, *Mater. Chem. Phys.* **2019**, *236*, 121724.
[69] Y. Lei, Y. Hao, H. Cheng, J. Ma, Y. Qin, Y. Kong, S. Komarneni, *Coll. Surf. A* **2021**, *628*, 127315.
[70] S. S. Suman, A. K. Ankita, N. Kataria, S. Kumar, P. Kumar, *J. Environ. Chem. Eng.* **2021**, *9*, 106266.
[71] A. Gomathi, T. Prabhuraj, S. Gokilapriya, G. Vasanthi, P. Maadeswaran, K. A. R. Kumar, *Dyes Pigm.* **2023**, *218*, 111473.
[72] Q. Guo, B. Zhang, Z. Yang, Q. Wang, Q. Wang, G. Wen, *Sep. Purif. Technol.* **2025**, *353*, 128448.
[73] Y. Gao, K. Chen, J. Ma, F. Gao, *Onco. Targets Ther.* **2014**, *7*, 835.
[74] G. Pulido-Reyes, I. Rodea-Palomares, S. Das, T. S. Sakthivel, F. Leganes, R. Rosal, S. Seal, F. Fernández-Piñas, *Sci. Rep.* **2015**, *5*, 15613.
[75] L. M. Bronstein, X. Huang, J. Retrum, A. Schmucker, M. Pink, B. D. Stein, B. Dragnea, *Chem. Mater.* **2007**, *19*, 3624.
[76] H. Gu, M. D. Soucek, *Chem. Mater.* **2007**, *19*, 1103.
[77] I. Kraljić, S. E. Mohsni, *Photochem. Photobiol.* **1978**, *28*, 577.

Manuscript received: January 16, 2025
Revised manuscript received: July 10, 2025
Version of record online: